Tailoring electronic and optical properties of TiO$_2$: nanostructuring, doping and molecular-oxide interactions

L. Chiodo[†], J. M. García-Lastra[†], D. J. Mowbray[†], A. Iacomino[‡], and A. Rubio[†,§]

[†]*Nano-Bio Spectroscopy group and ETSF Scientific Development Centre,*
Dpto. Física de Materiales, Universidad del País Vasco,
Centro de Física de Materiales CSIC-UPV/EHU- MPC and DIPC,
Av. Tolosa 72, E-20018 San Sebastián, Spain
[‡]*Dipartimento di Fisica "E. Amaldi", Università degli Studi Roma Tre,*
Via della Vasca Navale 84, I-00146 Roma, Italy
[§]*Friz-Haber-Institut der Max-Planck-Gesellschaft, Berlin, Germany*

1

Abstract

Titanium dioxide is one of the most widely investigated oxides. This is due to its broad range of applications, from catalysis to photocatalysis to photovoltaics. Despite this large interest, many of its bulk properties have been sparsely investigated using either experimental techniques or *ab initio* theory. Further, some of TiO_2's most important properties, such as its electronic band gap, the localized character of excitons, and the localized nature of states induced by oxygen vacancies, are still under debate. We present a unified description of the properties of rutile and anatase phases, obtained from *ab initio* state of the art methods, ranging from density functional theory (DFT) to many body perturbation theory (MBPT) derived techniques. In so doing, we show how advanced computational techniques can be used to quantitatively describe the structural, electronic, and optical properties of TiO_2 nanostructures, an area of fundamental importance in applied research. Indeed, we address one of the main challenges to TiO_2-photocatalysis, namely band gap narrowing, by showing how to combine nanostructural changes with doping. With this aim we compare TiO_2's electronic properties for 0D clusters, 1D nanorods, 2D layers, and 3D bulks using different approximations within DFT and MBPT calculations. While quantum confinement effects lead to a widening of the energy gap, it has been shown that substitutional doping with boron or nitrogen gives rise to (meta-)stable structures and the introduction of dopant and mid-gap states which effectively reduce the band gap. Finally, we report how *ab initio* methods can be applied to understand the important role of TiO_2 as electron-acceptor in dye-sensitized solar cells. This task is made more difficult by the hybrid organic-oxide structure of the involved systems.

PACS numbers:

I. INTRODUCTION

TiO_2 has been one of the most studied oxides over the past few years. This is due to the broad range of applications it offers in strategic fields of scientific, technological, environmental, and commercial relevance. In particular, TiO_2 surfaces and nanocrystals provide a rich variety of suitably tunable properties from structure to opto-electronics. Special attention has been paid to TiO_2's optical properties. This is because TiO_2 is regarded as one of the best candidate materials to efficiently produce hydrogen via photocatalysis[1,2]. TiO_2 nanostructures are also widely used in dye-sensitized solar cells, one of the most promising applications in the field of hybrid solar cells[1].

Since the first experimental formation of hydrogen by photocatalysis in the early 1980s,[2] TiO_2 has been the catalyst of choice. Reasons for this include the position of TiO_2's conduction band above the energy of hydrogen formation, the relatively long lifetime of excited electrons which allows them to reach the surface from the bulk, TiO_2's high corrosion resistance compared to other metal oxides, and its relatively low cost[1,3,4]. However, the large optical band gap of bulk TiO_2 ($\approx$ 3 eV) means that only high energy UV light may excite its electrons. This effectively blocks most of the photons which pierce the atmosphere, typically in the visible range, from participating in any bulk TiO_2 based photocatalytic reaction. On the other hand, the difference in energy between excited electrons and holes, i.e. the band gap, must be large enough ($\gtrsim$ 1.23 eV) to dissociate water into hydrogen and oxygen. For these reasons it is of great interest to adjust the band gap ε_{gap} of TiO_2 into the range $1.23 \lesssim \varepsilon_{gap} \lesssim 2.5$ eV, while maintaining the useful properties mentioned above[5].

With this aim, much research has been done on the influence of nanostructure[6–11] and dopants [5,11–19] on TiO_2 photocatalytic activity. For low dimensional nanostructured materials, electrons and holes have to travel shorter distances to reach the surface, allowing for a shorter quasi-particle lifetime. However, due to quantum confinement effects, lower dimensional TiO_2 nanostructures tend to have *larger* band gaps[20]. On the other hand, although doping may introduce mid-gap states, recent experimental studies have shown that boron and nitrogen doping of bulk TiO_2 yields band gaps *smaller* than the threshold for water splitting[12,13]. This suggests that low dimensional structures with band gaps larger than about 3.0 eV may be a better starting point for doping.

Recently, several promising new candidate structures have been proposed[11]. These small ($R \lesssim$ 5 Å) TiO_2 nanotubes, with a hexagonal ABC PtO_2 structure (HexABC), were found to be surprisingly stable, even in the boron and nitrogen doped forms. This stability may be attributed to their

structural similarity to bulk rutile TiO$_2$, with the smallest nanotube having the same structure as a rutile nanorod.

A further difficulty for any photocatalytic system is controlling how electrons and holes travel through the system [21]. For this reason, methods for reliably producing both n-type and p-type TiO$_2$ semiconducting materials are highly desirable. So far, doped TiO$_2$ tends to yield only n-type semiconductors. However, it has recently been proposed that p-type TiO$_2$ semiconducting materials may be obtained by nitrogen doping surface sites of low dimensional materials[11]. In this chapter we will discuss in detail the effects of quantum confinement and doping on the optical properties of TiO$_2$.

TiO$_2$ nanostructures are also one of the main components of hybrid solar cells. In a typical Grätzel cell[1], TiO$_2$ nanoparticles with average diameters around 20 nm collect the photoelectron transferred from a dye molecule adsorbed on the surface[22,23]. Such processes are favoured by a proper energy level alignment between solid and organic materials, although the dynamic part of the process also plays an important role in the charge transfer. Clearly, TiO$_2$'s characteristics of long quasi-particle lifetimes, high corrosion resistance, and relatively low cost, must be balanced with control of its energy level alignment with molecular states, and a fast electron injection at the interface.

Despite all the engineering efforts, the main scientific goal remains to optimize the efficiency of solar energy conversion into readily available electricity. Different research approaches have been devoted to benefit from quantum size properties emerging at the nanoscale[24,25], find an optimal donor-acceptor complex[24,25], mix nanoparticles and one-dimensional structures, such as nanotubes or nanowires[26,27], and control the geometry of the TiO$_2$ nano-assembly[28].

A clear theoretical understanding of TiO$_2$'s optoelectronic properties is necessary to help unravel many fundamental questions concerning the experimental results. In particular, the properties of excitons, photo-injected electrons, and surface configuration in TiO$_2$ nanomaterials may play a critical role in determining their overall behaviour in solar cells. For TiO$_2$ at both the nanoscale and macroscale regime, it is necessary to first have a complete picture of the optical properties in order to clarify the contribution of excitons.

Despite the clear importance of its surfaces and nanostructures, investigations of TiO$_2$ bulk (see 1) electronic and optical properties have not provided, so far, a comprehensive description of the material. Important characteristics,such as the electronic band gap, are still undetermined. Most of the experimental and computational work has been focused on synthesis and analysis of systems
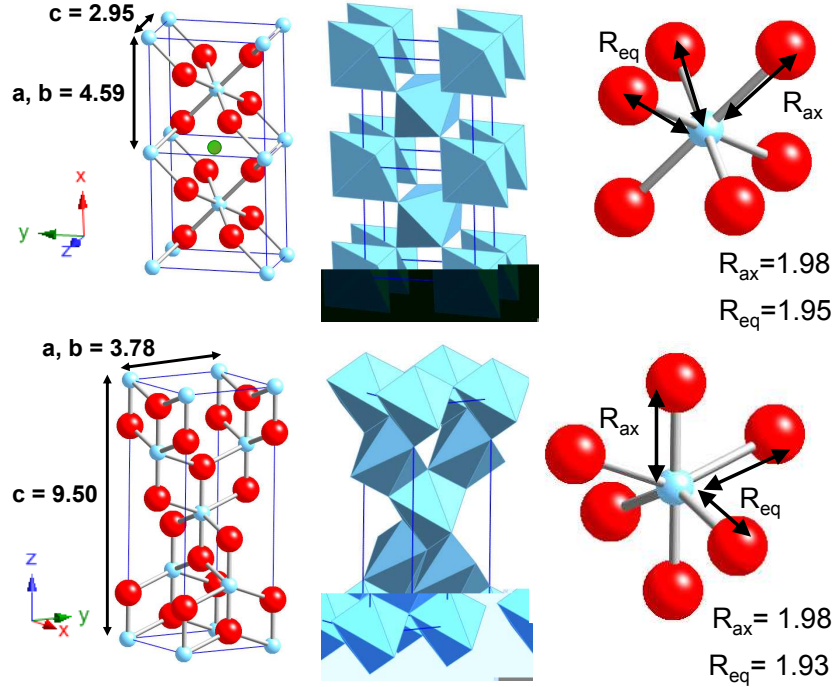
FIG. 1: Unit cell (left), crystallographic structure (center) and TiO_6 octahedrons (right) of rutile (top) and anatase (bottom). The lattice parameters in Å are denoted a, b, and c, while R_ax and R_eq are the distances in Å between a Ti^{4+} ion and its nearest and next-nearest neighbour O^{2-} ions, respectively. In the case of rutile the interstitial Ti impurity site is shown with a green circle (see left top).

with reduced dimensionality.

The experimental synthesis and characterization of nanostructured materials is in general a costly and difficult task. However, predictions of a dye or nanostructure's properties from simulations can prove a great boon to experimentalists. Modern large-scale electronic structure calculations have become important tools by providing realistic descriptions and predictions of structure and electronic properties for systems of technological interest.

Although it will not be treated in this chapter, it is important to mention the problem of electron localization in reduced titania[29]. This will provide a glimpse of the complexity faced, from the theoretical point of view, when studying transition metal atoms. The localization of d electrons makes the accurate description of their exchange–correlation interaction a difficult task[30]. The electron localization in defective titania has been an open question from both experimental and theoretical points of view, and caused much controversy during the past few years[31–33]. Oxygen vacancies are quite common in TiO_2, and their presence and behaviour can significantly affect

the properties of nanostructures. When an oxygen vacancy is created in TiO_2, i.e. when TiO_2 is reduced, the two electrons coming from the removed O^{2-} ion must be redistributed within the structure. One possibility is that these two extra electrons remain localized onto two Ti ions close to the O^{2-} vacancy. In this way a pair of Ti^{4+} ions become Ti^{3+} ions. Another option is for the two extra electrons to delocalize along the whole structure, i.e. they do not localize on any particular Ti ion. Finally, an intermediate situation, with one electron localized and the other spread, is also possible. Concerning the TiO_2 bulk, conventional density functional theory (DFT) calculations using either local density approximations (LDA) or generalized gradient approximations (GGA) for the exchange-correlation (xc)-functionals show a scenario with both electrons delocalized. On the other hand, hybrid functionals and Hartree-Fock calculations give rise to a situation with both electrons localized. For GGA+U calculations, the results are very sensitive to the value of the U parameter. For certain values of U both electrons remain localized, while for others there is an intermediate situation[34,35].

Experimentally, there are electron paramagnetic resonance (EPR) measurements suggesting that the extra electrons are mainly localized on interstitial Ti^{3+} ions[36]. These interstitial Ti^{3+} ions are impurities placed at the natural interstices of the rutile lattice (see 1) and, similarly to the Ti^{4+} ions of the pure lattice, they also form TiO_6 octahedrons. Recent STM and PES experiments have shown that the interstitial Ti^{3+} ions play a key role in the localization of the electrons when a bridge oxygen is removed from the TiO_2 (110) surface[37]. These experiments concluded the controversial discussion about the localization of electrons in the bridge oxygen defective TiO_2 (110) surface (see Refs.[31–33] for more details). However, the problem remains unresolved for the bulk case.

In summary, in this chapter we first analyze the full *ab initio* treatment of electronic and optical properties in II and III, before applying it to the two most stable bulk phases, rutile and anatase in IV. These are also the phases most easily found when nanostructures are synthesized. We will focus on their optical properties and excitonic behaviour. We then explore the possibility of tuning the oxide band gap using quantum confinement effects and dimensionality, by analyzing atomic clusters, nanowires and nanotubes in V. A further component whose effect has to be evaluated is that of doping, which may further tune the optical behaviour by introducing electronic states in the gap, as presented in VI.Combining the effects of quantum confinement and doping is hoped to produce a refined properties control. In VII, we report some details on modeling for dye-sensitized solar cells, before providing a summary and our concluding remarks.

II. GROUND STATE PROPERTIES THROUGH DENSITY FUNCTIONAL THEORY

DFT is a many-body approach, successfully used for many years to calculate the ground-state electronic properties of many-electron systems. However, DFT is by definition a ground state theory, and is not directly applicable to the study of excited states. To describe these types of physical phenomena it becomes necessary to include many-body effects not contained in DFT through Green's function theory. The use of many-body perturbation theory[38], with DFT calculations as a zero order approximation, is an approach widely used to obtain quasi-particle excitation energies and dielectric response in an increasing number of systems, from bulk materials to surfaces and nanostructures. We present a short, general discussion of the theoretical framework, referring the reader to the books and the reviews available in the literature for a complete description (see, for instance, Refs.[39] and[40]), before applying these methods to rutile and anatase TiO_2.

As originally introduced by Hohenberg and Kohn (HK) in 1964[41], DFT is based on the theorem that the ground state energy of a system of N interacting electrons in an external potential $V_{ext}(\mathbf{r})$ is a unique functional of the ground state electronic density. The Kohn and Sham[42] formulation demonstrates how the the HK Theorem may be used in practice, by self-consistently solving a set of one-electron equations (KS equations),

$$\left[-\frac{1}{2}\nabla^2 + V_{eff}^{KS}[\rho(\mathbf{r})]\right]\phi_i(\mathbf{r}) = \varepsilon_i^{KS}\phi_i(\mathbf{r}), \quad \rho(\mathbf{r}) = \sum_i^N |\phi_i(\mathbf{r})|^2, \tag{1}$$

where $\rho(\mathbf{r})$ is the electronic charge density, $\phi_i(\mathbf{r})$ are the non-interacting KS wavefunctions, and $V_{eff}^{KS}[\rho(\mathbf{r})] = V_{ext}(\mathbf{r}) + V_H[\rho(\mathbf{r})] + V_{xc}[\rho(\mathbf{r})]$ is the effective one-electron potential. Here, V_H is the Hartree potential and V_{xc} is the exchange–correlation potential defined in terms of the xc-functional E_{xc} as $V_{xc} = \frac{\delta E_{xc}}{\delta\rho(r)}$, which contains all the many-body effects. V_{xc} is usually calculated in either LDA[43,44] or GGA[45] approximations. However, semi-empirical functionals are also available, called hybrids[46,47], which somewhat correct the deficiencies of LDA and GGA for describing exchange and correlation. This is accomplished by including an exact exchange contribution.

Other than the highest occupied molecular orbital (HOMO), KS DFT electronic levels do not correspond to the electronic energies of the many electron system. Indeed, the calculated KS band gaps of semiconductors and insulators severely underestimate the experimental ones. Experimentally, occupied states are accessible by direct photoemission, where an electron is extracted from the system ($N-1$ ground state), while unoccupied states are accessible by inverse photoemission, where one electron is added to the system ($N+1$ ground state). For isolated systems with a finite

number of electrons, the electronic gap may be obtained from the DFT calculated ground-state energies with $N + 1$, N, and $N − 1$ electrons[48]. However, for periodic systems, adding or removing an electron is a non-trivial task. We therefore summarize in the following a rigorous method for describing excitations based on the Green's function approach. This method allows us to properly describe the electronic band structure. Further information and details about the Green's function approach may be found elsewhere[40,49–51].

III. EXCITED STATES WITHIN MANY BODY PERTURBATION THEORY

When a bare particle, such as an electron or hole, enters an interacting system, it perturbs the particles in its vicinity. In essence, the particle is "dressed" by a polarization cloud of the surrounding particles, becoming a so-called quasi-particle. Using this concept, it is possible to describe the system through a set of quasi-particle equations by introducing a non-local, time-dependent, non-Hermitian operator called the self-energy Σ. This operator takes into account the interaction of the particle with the system via

$$\left[-\frac{1}{2}\nabla^2 + V_{ext} + V_H \right] \Psi_i(\mathbf{r}, \omega) + \int \Sigma(\mathbf{r}, \mathbf{r}', \omega)\Psi_i(\mathbf{r}', \omega)d\mathbf{r}' = E_i(\omega)\Psi_i(\mathbf{r}), \tag{2}$$

where $\Psi_i(\mathbf{r})$ is the quasi-particle wavefunction.

Since the operator Σ is non-Hermitian, the energies $E_i(\omega)$ are in general complex, and the imaginary part of Σ is related to the lifetime of the excited particle[52]. The most often used approximation to calculate the self-energy is the so-called GW method. It may be derived as the first-step iterative solution of the Hedin integral equations (see Refs.[38],[53], and[54]), which link the Green's function G, the self-energy Σ, the screened Coulomb potential W, the polarization P and the vertex Γ. In practice 2 is not usually solved directly, since the KS wavefunctions are often very similar to the GW ones[53]. For this reason it is often sufficient to calculate the quasi-particle (QP) corrections within first-order perturbation theory (G_0W_0) [53,54]. Moreover, the energy dependence of the self-energy is accounted for by expanding Σ in a Taylor series, so that the QP energies $\varepsilon_i^{G_0W_0}$ are then given by

$$\varepsilon_i^{G_0W_0} = \varepsilon_i^{KS} + Z_i\langle\phi_i^{KS}|\Sigma(\varepsilon_i^{KS}) - V_{xc}^{KS}|\phi_i^{KS}\rangle, \tag{3}$$

where Z_i are the quasi-particle renomalization factors described in Refs.[40] and[49]. For a large number of materials, the G_0W_0 approximation of Σ works quite well at correcting the KS electronic gap from DFT.

Concerning optical properties, the physical quantity to be determined in order to obtain the optical spectra is the macroscopic dielectric function $\epsilon_M(\omega)$. This may be calculated at different levels of accuracy within a theoretical *ab initio* approach. A major component in the interpretation of the optical measurements of reduced dimensional systems are the local-field effects (LFE). These effects are especially important for inhomogeneous systems. Here, even long wavelength external perturbations produce microscopic fluctuations of the electric field, which must be taken into account. However, LFE are also important for bulk phases such as anatase and rutile TiO_2. They must be taken into account in the evaluation of optical absorption, and to calculate the screened interaction W used in GW. The effect becomes increasingly important when going to lower dimensional systems.

It is well known[55] that for inhomogeneous materials $\epsilon_M(\omega)$ is not simply the average of the corresponding microscopic quantity, but is related to the inverse of the microscopic dielectric matrix by

$$\epsilon_M(\omega) = \lim_{\mathbf{q}\to 0} \frac{1}{\epsilon^{-1}_{\mathbf{G}=0,\mathbf{G}'=0}(\mathbf{q},\omega)}. \tag{4}$$

The microscopic dielectric function may be determined within the linear response theory[56], the independent-particle picture by the random phase approximation (RPA), and using eigenvalues and eigenvectors of a one-particle scheme such as DFT or GW. There is also a different formulation which includes LFE in the macroscopic dielectric function. This becomes useful when the electron–hole interaction is included in the polarization function. This formulation allows us to include, via the Bethe-Salpeter equation (BSE), excitonic and LFE on the same footing. In so doing, inverting of the microscopic dielectric matrix is avoided. The complete derivation may be found in Appendix B of Ref.[57].

So far, in RPA, we have treated the quasi-particles as non-interacting. To take into account the electron–hole interaction, a higher order vertex correction needs to be included in the polarization. In other words, the BSE, which describes the electron–hole pair dynamics, needs to be solved. As explained in Ref.[57], the BSE may be written as an eigenvalue problem involving the effective two-particle Hamiltonian

$$\begin{aligned} H^{(n_1,n_2),(n_3,n_4)}_{exc} &= (E_{n_2} - E_{n_1})\delta_{n_1,n_3}\delta_{n_2,n_4} - i(f_{n_2} - f_{n_1}) \\ &\times \int d\mathbf{r}_1 \, d\mathbf{r}'_1 \, d\mathbf{r}_2 \, d\mathbf{r}'_2 \; \phi_{n_1}(\mathbf{r}_1) \, \phi^*_{n_2}(\mathbf{r}'_1) \, \Xi(\mathbf{r}_1, \mathbf{r}'_1, \mathbf{r}_2, \mathbf{r}'_2) \, \phi^*_{n_3}(\mathbf{r}_2) \, \phi_{n_4}(\mathbf{r}'_2). \end{aligned}$$

The kernel Ξ contains two contributions: $\bar{v}$, which is the bare Coulomb interaction with the long

range part corresponding to a vanishing wave vector not included and W, the attractive screened Coulomb electron–hole interaction. Using this formalism and considering only the resonant part of the excitonic Hamiltonian[57], the macroscopic dielectric function may be expressed as[57]

$$\epsilon_M(\omega) = 1 + \lim_{\mathbf{q} \to 0} v(\mathbf{q}) \sum_\lambda \frac{\left| \sum_{v,c;\mathbf{k}} \langle v, \mathbf{k} - \mathbf{q} | e^{-i\mathbf{q}\mathbf{r}} | c, \mathbf{k} \rangle A_\lambda^{(v,c;\mathbf{k})} \right|^2}{(E_\lambda - \omega)}. \tag{5}$$

In 5 the dielectric function, differently from the RPA approximation, is given by a mixing of single particle transitions weighted by the excitonic eigenstates A_λ. These are obtained by the diagonalization of the excitonic Hamiltonian. Moreover, the excitation energies in the denominator are changed from $\epsilon_c - \epsilon_v$ to E_λ. The electronic levels are mixed to produce optical transitions, which are no longer between pairs of independent particles. The excitonic calculation is in general, from the computational point of view, very demanding because the matrix to be diagonalized may be very large. The relevant parameters which determine its size are the number of $\mathbf{k}$-points in the Brillouin zone, and the number of valence and conduction bands, N_v and N_c respectively, which form the basis set of pairs of states.

Calculations performed for insulators and semiconductors show that the inclusion of the electron–hole Coulomb interaction yields a near-quantitative agreement with experiment. This is not only true below the electronic gaps, where bound excitons are generally formed, but also above the continuum edge. The same results apply to the titania-based materials investigated here, as shown in the following section.

IV.   THE BULK PHASES OF TIO$_2$: ROLE OF MANY BODY EFFECTS

Despite the importance of its surfaces and nanostructures, the most recent measurements of TiO$_2$'s bulk (see Fig. 1) electronic and optical properties were performed in the 1960s, with a few exceptions. Here we aim to review the existing results obtained using a variety of experimental techniques and *ab initio* calculations, in order to elucidate the known properties of TiO$_2$. Previous data will be compared with a complete, consistent *ab initio* description, which includes many body effects when describing electronic and optical properties. Most experimental and theoretical data reported refers to the rutile phase, while anatase in general has been less studied. However, anatase has received more attention recently, due in part to its greater stability at the nanoscale compared to rutile.

10

As we will see, while a general agreement seems to exist concerning the optical absorption edge of these materials, values for basic electronic properties such as the band gap still have a large degree of uncertainty.

The electronic properties of valence states of rutile TiO_2 have been investigated experimentally by angle-resolved photoemission spectroscopy[58], along the two high symmetry directions (Δ and Σ) in the bulk Brillouin zone. The valence band of TiO_2 consists mainly of O $2p$ states partially hybridized with Ti $3d$ states. The metal $3d$ states constitute the conduction band, with a small amount of mixing with O $2p$ states. This photoemission data was compared to calculations performed with both pseudopotentials and linear muffin-tin orbital (LMTO) methods, which gave a direct gap of 2 eV in both cases. On the other hand, within the linear combination of atomic orbitals (LCAO) method, a gap of 3 eV was obtained.

From the symmetry of the TiO_6 octahedrons (see 1), d states are usually grouped into low energy t_{2g} and high energy e_g sub-bands. It is important to note that, from ultraviolet photoemission spectroscopy (UPS) data, it has been deduced that the electronic gap for rutile is at least 4 eV. This is the observed binding energy of the first states below the Fermi energy. This is in agreement with previous reported data from electron energy loss spectroscopy[59], and from other UPS[60–62] results. The electronic structure of rutile bulk has also been described using other experimental techniques, such as electrical resistivity[63], electroabsorption[64,65], photoconductivity and photoluminescence[66,67], X-ray absorption spectroscopy (XAS)[68–73], resonant Raman spectra[67,74] photoelectrochemical analysis[75,76] and UPS[77]. All of these experiments have provided many important details of its electronic properties, in particular concerning the hybridization between Ti $3d$ and O $2p$ states. However, the electronic band gap, corresponding to the difference between the valence band maximum (VBM) and the conduction band minimum (CBM), has not been obtained directly from any experimental data. Although the electronic band gap could be measured using combined photoemission and inverse photoemission experiments, such experiments do not appear in the literature.

The same discussion is valid for the anatase crystalline phase. Even though there are several XAS measurements concerning its electronic structure[73,78,79], photoemission data is completely lacking for anatase. In the absence of more recent and refined experimental results for rutile, and due to the lack of results for anatase, we are left with an estimate of 4 eV for the electronic gap of rutile TiO_2. It is this value which we shall use as a reference in the following discussion.

We will now review the experimental results for optical properties of TiO_2. Such measurements

are of great interest for the photocatalytic and photovoltaic applications of this material. From the optical absorption spectra of both phases[80], the room temperature optical band gap is found to be 3.0 eV for rutile, and 3.2 eV for anatase.

The absorption edge has been investigated in detail for rutile by combining absorption, photoluminescence, and Raman scattering techniques[81]. These techniques provide a value for the edge of 3.031 eV associated to a $2p_{xy}$ exciton, while a lower energy $1s$ quadrupolar exciton has been identified below 3 eV. The first dipole allowed gap is at 4.2 eV[81] according to the combined results of these three techniques. Concerning anatase[82,83], the optical spectrum have been recently re-evaluated[83], confirming the 3.2 eV value for the edge. The fine details of anatase's spectrum have also been recently investigated[84]. Data on the Urbach tail has revealed that excitons in anatase are self-trapped in the octahedron of coordination of the titanium atom. This is in contrast to the rutile phase, where excitons are known to be free due to the different packing of rutile's octahedra.[84]

In general, measurements of optical properties can be significantly affected by the presence of defects, such as oxygen vacancies, and by phonons. Both defects and phonons will be present in any experimental sample of the material at finite temperatures. These observations have to be kept in mind when directly comparing experimental measurements with the theoretical results presented in the following. Moreover, there is a general trend in theoretical-computational studies to compare the theoretical electronic band gaps with the experimental optical gap values[29,85,85–88] derived from the above mentioned experiments.

It should be remembered that almost by definition, the optical gap is always smaller than the electronic band gap. This is because the two types of experiments (photoemission, and optical absorption) provide information on two different physical quantities. Reverse photoemission experiments involve a change in the total number of electrons in the material ($N \rightarrow N + 1$), while optical absorption experiments do not ($N \rightarrow N^*$). The latter involves the creation of an electron–hole pair in the material, with the hole stabilizing the excited electron. For this reason, comparison between experimental and theoretical data, and the resulting discussion, must take into account the proper quantities.

The theoretical investigations presented in the literature of TiO_2's structural, electronic, and optical properties are at varying levels of theory and thus somewhat inconsistent. A comprehensive description of properties of both phases in the same theoretical and computational framework is still missing. Here we present, in a unified description and by treating with the same method for the two phases, the electronic and optical properties of the two most stable phases of bulk titania.

The *ab intio* calculations performed yield results[89] in quite good agreement with the few available pieces of experimental data.

A combination of DFT[41] and many body perturbation theory (MBPT) methods is a reliable and well established toolkit to obtain a complete analysis of electronic and optical properties for a large class of materials and structures. In this DFT $+ GW +$ BSE framework, the properties of the two bulk phases of TiO_2 may be properly analyzed. Their structural and energetic properties have been calculated[89] using DFT, as a well established tool for the description of ground state properties. However, the DFT gap is, as expected, significantly smaller than the experimental gap, with the relative positions of the s, p, and d levels also affected by this description. To address this, standard G_0W_0 calculations may be applied to obtain the quasi-particle corrections to the energy levels, starting from DFT eigenvalues and eigenfunctions. Finally the electron–hole interaction is included, to properly describe the optical response of the system.

The description of ground state properties[86,90] performed in the framework of DFT are generally quite good, with the structural description of TiO_2 systems in reasonable agreement with experiments[89]. The lattice constants are within 2% of experiment, while bulk modulii are within 10% of the experimental results[86,90], as is often found for DFT. However, DFT incorrectly predicts the anatase phase to be more stable than the rutile one, even for a small energy difference, independently of the xc-functional used[86].

Even if DFT is not an excited state method, the KS wavefunctions are often used to evaluate the band structure along the high symmetry directions (*cf.* 2 for rutile), the density of states, and the spatial behaviour of wavefunctions involved in the relevant bonds in the system[58,89,91,92]. The KS electronic gap, corresponding to the difference between the VBM and the CBM, is 1.93 eV and 2.16 eV for rutile (direct gap) and anatase (indirect gap), respectively. These are underestimations by almost 2 eV of the available experimental data[58]. However, the overall behaviour of the band dispersion of KS levels is reasonable, with valence bands mainly given by O $2p$ states, and Ti $3d$ states forming the conduction bands.

The application of standard GW methods gives gaps of 3.59 and 3.97 eV for rutile and anatase[89], respectively. The value for rutile is again smaller than the one given by the UPS estimation[58], but still close to the experimental value of 4 eV.

There exist a number of theoretical works, with calculations performed at different levels of DFT or including MBPT descriptions, for the electronic gap of rutile and anatase TiO_2[85,85,87,91–94]. Therefore in literature it is possible to find for the electronic gap a quite large range of possible
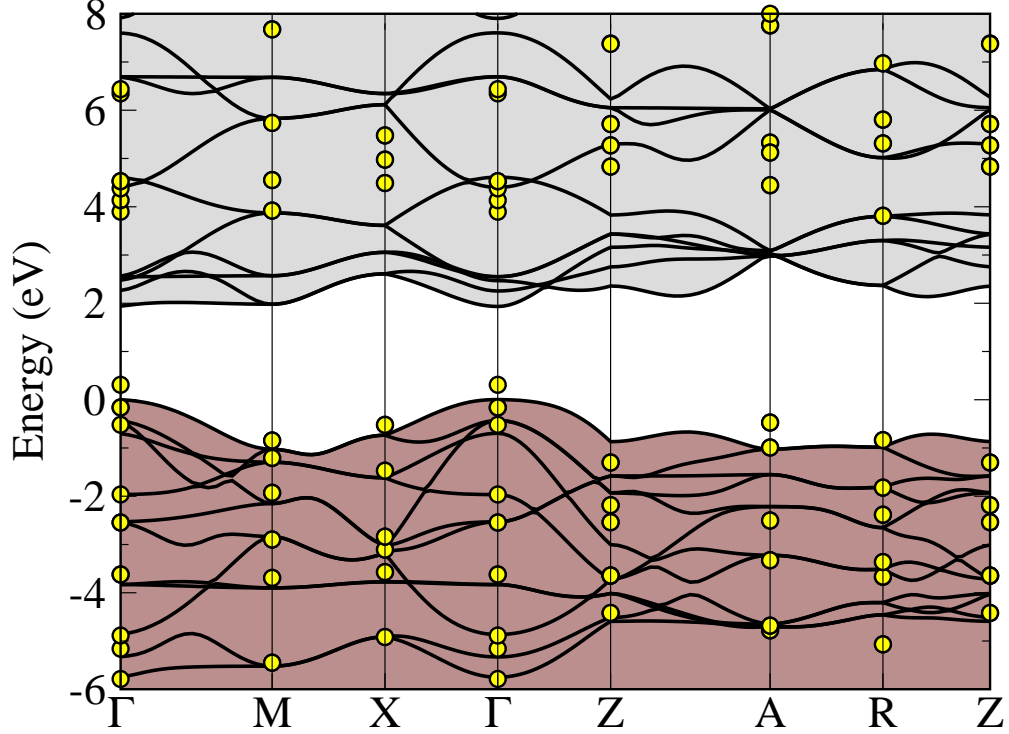
FIG. 2: Electronic band structure of rutile bulk, along the high symmetry directions of the irreducible Brillouin zone, from GGA calculations (——). and including the G_0W_0 correction ($\bullet$).

values, attributed to the gap of titanium dioxide, which are often erroneously compared with the experimental optical gap.

The DFT-GGA values calculated[89] are comparable to the ones obtained with a variety of different DFT approaches, with different functionals, by using plane waves or localized basis methods, and all-electron or pseudopotential approaches. Only the hybrid PBE0[46] and B3LYP[47] xc-functionals give larger values.

From quasi-particle calculations, the electronic gap of anatase has been estimated to be 3.79 eV[94] by G_0W_0. However the more refined computational approach, because of its inclusion of a self-consistent evaluation of GW, yields a gap of 3.78 eV for rutile TiO_2.[85,85]

Moving to optical properties, and by applying the RPA method to both KS and QP energies, we obtain spectra (Fig. 3) that do not in overall behaviour agree with experiment. Differences are clear both in absorption edge determination, and in the overall shape of the spectra. The inclusion of quasi-particle corrections at the GW level yields a rigid shift of the absorption spectrum, moving the edge at higher energies, due to the opening of the gap. However, the shape of the absorption is quite unaffected, because the interaction is still treated using an independent quasi-
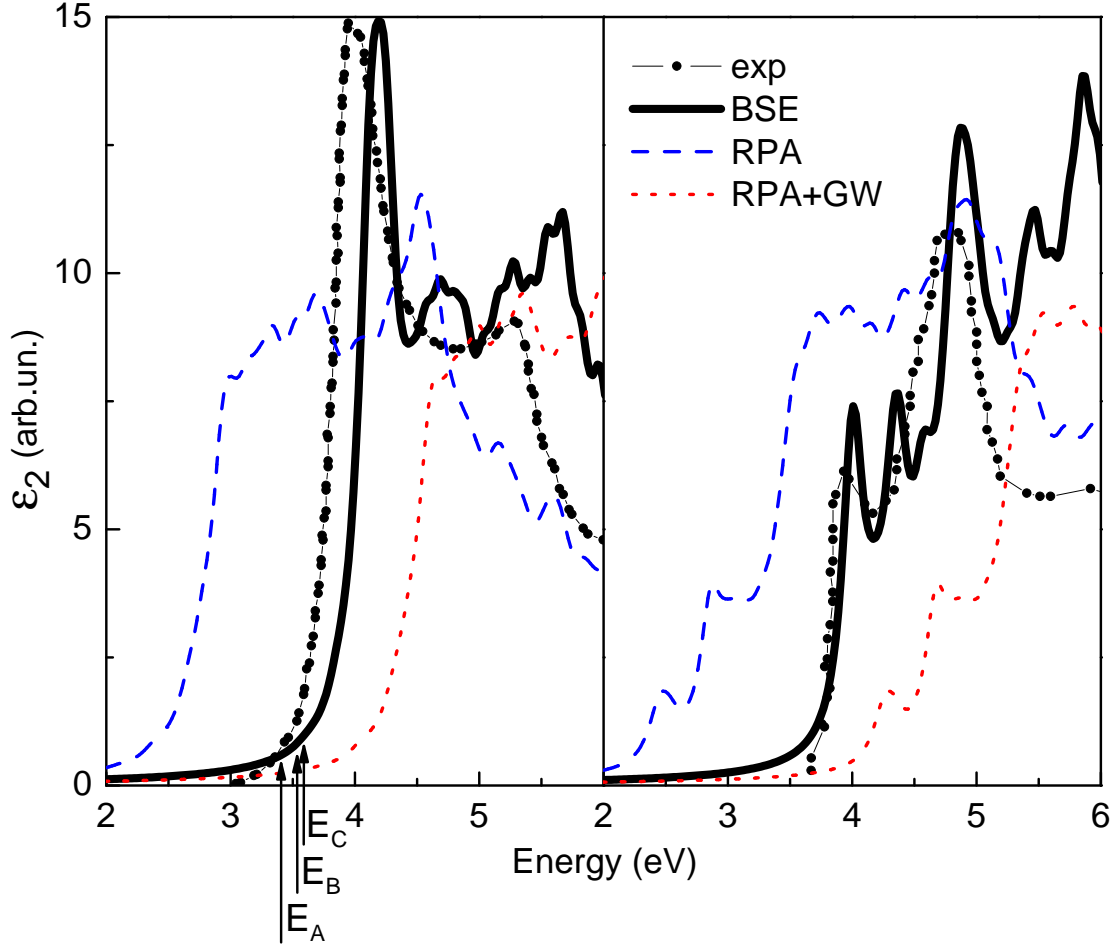
FIG. 3: Imaginary part of the dielectric constant for rutile (left), and anatase (right), in-plane polarization, calculated by GGA RPA (– – –), using G_0W_0 on top of GGA (· · · · · ·), and via the Bethe-Salpeter equation (BSE) (——). The experimental spectrum (— • —) from Refs.[80] and[92] is also shown for comparison.

particle approximation. A substantially better agreement may be obtained[89,95] by solving the BSE, which takes into account both many body interactions and excitonic effects. Indeed, it produces a good description of absorption spectra and excitons, as shown in Fig. 3

The optical absorption spectra calculated for the two phases, with polarization along the x-direction of the unit cells, are provided in 3. The spectra given by independent-particle transitions present two characteristic features. First, the band edge is underestimated, due to the electronic gap underestimation in DFT. Second, the overall shape of the spectrum is, for both phases, and both orientations, different from the experiment, in the sense that the oscillator strengths are not correct. The inclusion of the quasi-particle description, which should improve the electronic gap description, does not improve the overall shape of the spectrum. The absorption edge is, however,
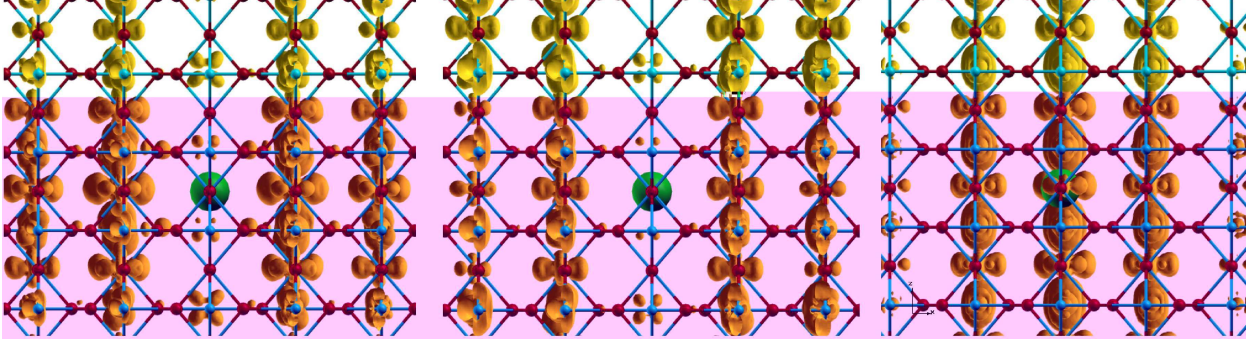
FIG. 4: Spatial distribution (yellow isosurfaces in arbitrary units) of the partial dark, dark, and optically active first three excitons in rutile. The hole position is denoted by the light green dot.

shifted at higher energies, even higher than expected from experiments. The description of optical properties within the two interacting quasi-particle approximation (by solving the BSE) definitely improves the results. The absorption edge is now comparable to the experimental one, with the optical gap estimated from our calculations in good agreement with the available data. Further, the shape of the spectrum is now well described, with a redistribution of transitions at lower energies. The agreement is generally good for both phases[89].

The nature of the exciton is still under debate in TiO_2 materials[89]. The experimental binding energy is of 4 meV and some uncertainty exists for the exact determination of optical edge. Moreover, the exciton is localized in one of the two phases, and delocalized in the other one, at least based on experimental results. However, an explanation for this behaviour is so far missing. Refined measurements[67] give an exciton of $2p_{xy}$ character at 3.031 eV, and a $1s$ quadrupolar exciton at energy lower than 3 eV. From *ab initio* calculations with x polarization, two dark (optically inactive) or quasi dark excitons are located in rutile at 3.40 and 3.55 eV (denoted by E_A, E_B in 4). At the same time, the optically active exciton, with 4 meV of binding energy, is located at 3.59 eV (E_C in 4). The spatial distribution of the first three excitons is plotted in 4. The transitions are from O $2p$ states to Ti $3d$ states of the triplet t_{2g}, as expected. While the first two optically forbidden transitions involve Ti atoms farther away from the excited O atom, the optical active transition involves states of the nearest neighbour Ti atoms.

In this section we have endeavoured to clarify though the application of a consistent description, the properties of the two main crystalline phases of titania. Particular attention has been taken to how the inclusion of a proper description of exchange and correlation effects can improve the description of both electronic and optical properties of TiO_2.

Now that bulk properties are known, from a theoretical point of view, at the level that the state-of-the-art *ab initio* techniques allow us to reach, we can attempt to describe how quantum confinement induced by reduced dimensionality, and doping both effect the properties of TiO_2. Our final aim is to demonstrate how we may tune the electronic and optical gap of nanostructures for photocatalytic and photovoltaic applications.

V. USING NANOSTRUCTURE TO TUNE THE ENERGY GAP

Having described in the previous section the electronic structure of the two bulk TiO_2 phases, we will now turn our attention to the influence of nanostructure on the energy gap. This is an area which has received considerable attention in recent years[6–11], in part due to the inherently high surface to volume ratio of nanostructures. It is hoped that this will allow materials with shorter quasi-particle lifetimes to function effectively for photocatalytic activities, since excitons are essentially formed at the material's surface. However, this advantage is partly countered by quantum confinement effects, which tend to increase the energy gap in nanostructures. These competing factors make the accurate theoretical determination of energy gaps in nanostructured materials a thing of great interest.

However, as shown in the previous section, standard DFT calculations tend to underestimate electronic band gaps for bulk TiO_2 by approximately 2 eV, due in part to self-interaction errors[96,97]. These errors arise from an incomplete cancellation of the electron's Coulomb potential in the exchange-correlation (xc)-functional.

This may be partially addressed by the use of hybrid functionals such as B3LYP[47], which generally seem to improve band gaps for bulk systems[32,87,98]. However, such calculations are computationally more expensive, due to the added dependence of the xc-functional on the electron's wavefunction. Moreover, B3LYP calculations for TiO_2 clusters largely underestimate the gap relative to the more reliable difference between standard DFT calculated ionization potential I_p and electron affinity E_a. For isolated systems such as clusters, the needed energetics of charged species are quantitatively described by standard DFT. Also, B3LYP and RPBE[99] calculations provide the same qualitative description of the *trends* in the energy gaps for TiO_2, as seen in 5. Another methodology is thus needed to describe the band gaps of periodic systems.

G_0W_0 is probably the most successful and generally applicable method for calculating quasi-particle gaps. For clusters it agrees well with $I_p - E_a$, and it has been shows to produce reliable
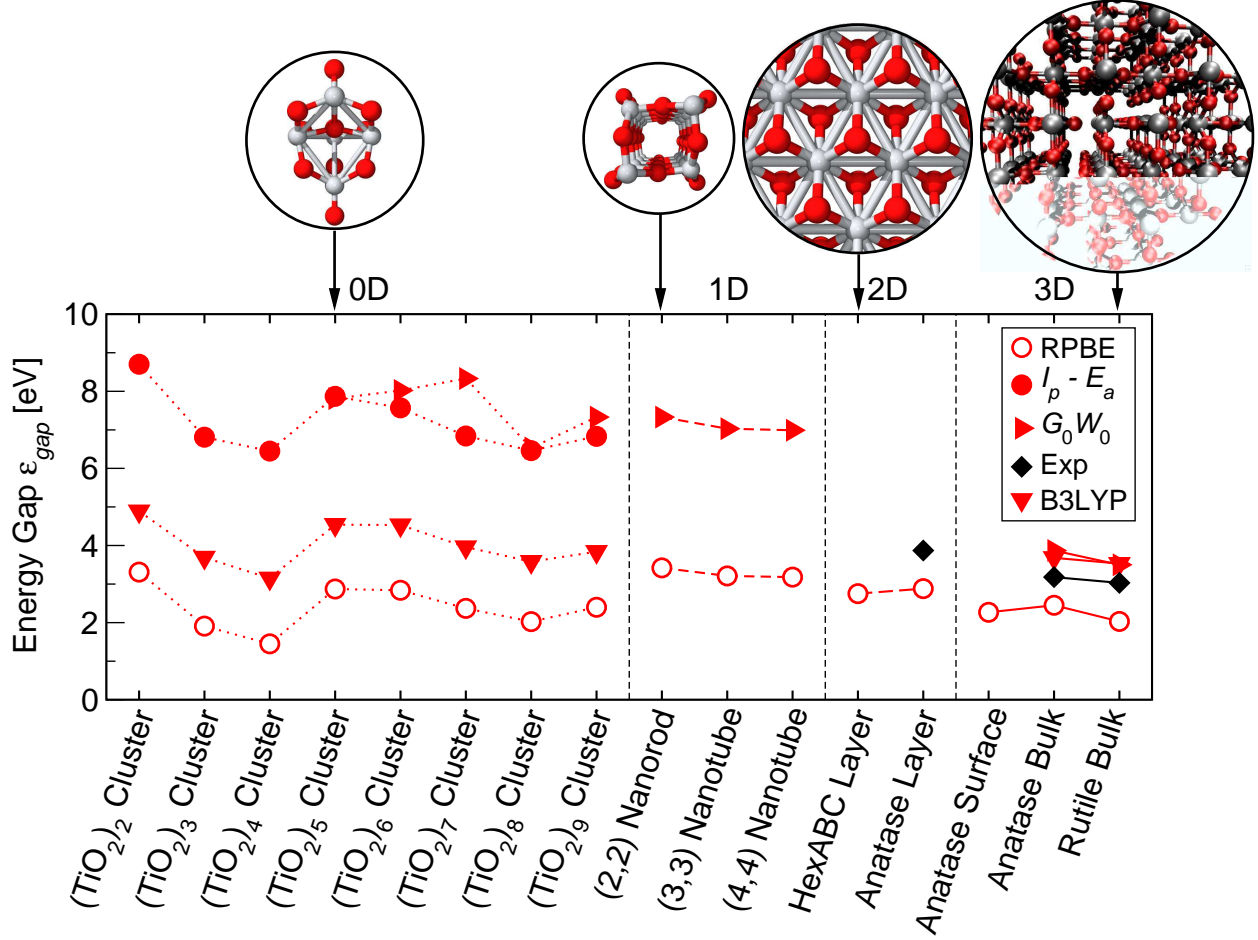
FIG. 5: Energy gap ε_{gap} in eV versus TiO$_2$ structure for 0D (TiO$_2$)$_n$ clusters ($n \leq 9$), 1D TiO$_2$ (2,2) nanorods, (3,3) nanotubes, (4,4) nanotubes, 2D HexABC and anatase layers, and 3D anatase surface, anatase bulk, and rutile bulk phases. DFT calculations using the highest occupied and lowest unoccupied state gaps with the standard GGA RPBE xc-functional (○) and the hybrid B3LYP xc-functional (▼), are compared with DFT $I_p - E_a$ calculations (●), G_0W_0 quasi-particle calculations (▶), and experimental results (◆)[6,11,13,20,94]. Schematics of representative structures for each dimensionality are shown above and taken from Ref.[11].

results for bulk phases. On the other hand, G_0W_0 calculations describe an $N \rightarrow N+1$ transition where the number of charges is not conserved, rather than the electron–hole pair induced by photoabsorption, which is a neutral process. Indeed, a description in terms of electronic gap cannot be compared with, or provide direct information on the optical gap, which is the most investigated quantity, due to its critical importance for photocatalytic processes.

5 shows that for both 3D and 2D systems, RPBE gaps underestimate the experimental optical

gaps by approximately 1 eV. For 1D and 0D systems, there is a much larger difference of about 4 eV and 5 eV respectively, between the RPBE gaps and the $I_p - E_a$ and G_0W_0 results. This increasing disparity may be attributed to the greater quantum confinement and charge localization in the 1D and 0D systems, which yield greater self-interaction effects. The B3LYP gaps also tend to underestimate this effect, simply increasing the RPBE energy gaps for both 0D and 3D systems by about 1.4 eV.

On the other hand, the RPBE gaps reproduce qualitatively the structural dependence of the $I_p - E_a$, G_0W_0, and experimental results for a given dimensionality, up to a constant shift. This is true even for 3D bulk systems, where standard DFT does not correctly predict rutile to be the most stable structure[86].

To summarize, quantum confinement effects seem to increase the energy gap significantly for both 0D and 1D systems, while 2D and 3D systems may be much less affected. This suggests that 2D laminar structures are viable candidates for reducing the minimal quasi-particle, while leaving the band gap nearly unchanged. However, a more accurate description of the photoabsorption properties of these novel nanostructures, perhaps using the methodologies recently applied to bulk TiO_2[89], still remains to be found.

VI. INFLUENCE OF BORON AND NITROGEN DOPING ON TIO$_2$'S ENERGY GAP

The doping of TiO_2 nanostructures has received much recent attention as a possible means for effectively tuning TiO_2's band gap into the visible range[5,11–19]. Recent experiments suggest substituting oxygen by boron or nitrogen in the bulk introduces mid-gap states, allowing lower energy excitations. However, to model such systems effectively requires large supercells, both to properly describe the experimental doping fractions of $\lesssim 10\%$, and to ensure dopant–dopant interactions are minimized.

6 shows the DFT calculated DOS and structures for the most stable boron doped and nitrogen doped TiO_2 (2,2) nanorods. The highest occupied state is also shown as isosurfaces of $\pm 0.05 e/\text{Å}^3$ in the side views of the doped structures.

As with TiO_2 clusters, the influence of boron dopants on TiO_2 nanorods may be understood in terms of boron's weak electronegativity, especially when compared with the strongly electronegative oxygen. Boron prefers to occupy oxygen sites which are 2-fold coordinated to neighbouring titanium atoms. However, as with the 0D clusters, boron's relatively electropositive character
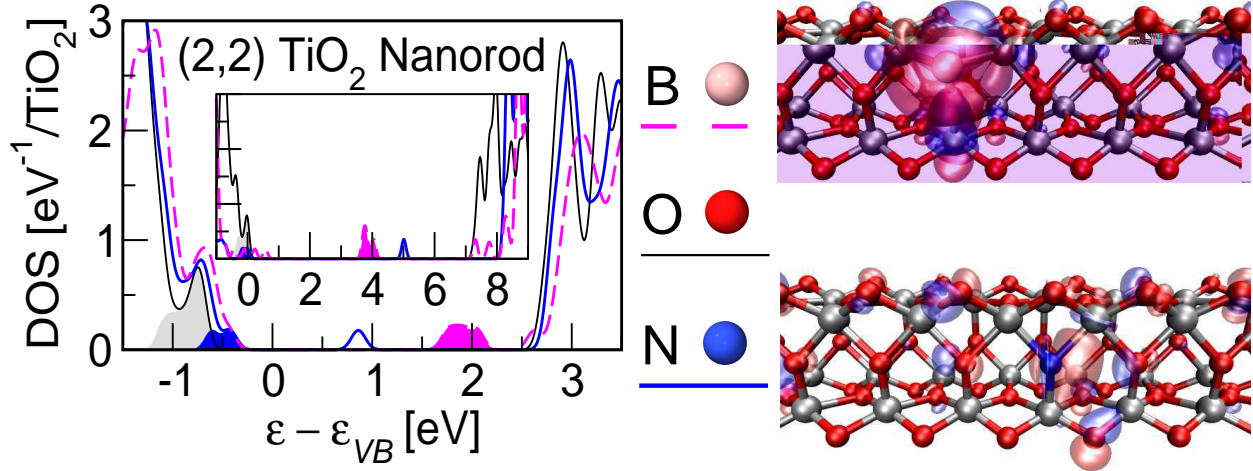
FIG. 6: Total density of states (DOS) in eV^{-1} per TiO_2 functional unit vs. energy ε in eV for undoped (——), boron doped (– – –) and nitrogen doped (——) (2,2) TiO_2 nanorods from standard DFT GGA RPBE xc-functional and (inset) G_0W_0 quasi-particle calculations. The highest occupied states for boron and nitrogen doped (2,2) TiO_2 nanorods are depicted by isosurfaces of $\pm 0.05e/\text{Å}^3$ in the structure diagrams to the left.

induces significant structural changes in the 1D structures, creating a stronger third bond to a neighbouring three-fold coordinated oxygen via an oxygen dislocation, as shown in 6. This yields three occupied mid-gap states localized on the boron dopant, which overlap both the valence band O $2p_\pi$ and conduction band Ti $3d_{xy}$ states, as shown in 6. Boron dopants thus yield donor states near the conduction band, which may be photocatalytically active in the visible region. However, the quantum confinement inherent in these 1D structures may stretch these gaps, as found for the G_0W_0 calculated DOS shown in the inset of 6.

On the other hand, nitrogen dopants prefer to occupy oxygen sites which are 3-fold coordinated to Ti, as was previously found for the rutile TiO_2 surface[17,18]. This yields one occupied state at the top of the valence band and one unoccupied mid-gap state in the same spin channel. Both states are localized on the nitrogen dopant but overlap the valence band O $2p_\pi$ states, as shown in 6. Nitrogen dopants thus act as acceptors, providing localized states well above the valence band, as is also found for the G_0W_0 calculated DOS shown in the inset of 6.

Although nitrogen dopants act as acceptors in TiO_2 1D structures, such large gaps between the valence band and the unoccupied mid-gap states would not yield p-type semiconductors. This may be attributed to the substantial quantum confinement in these 1D structures. However, for 2D and 3D systems, it is possible to produce both p-type and n-type classical semiconductors, as

discussed in Ref.[11]. This has recently been shown experimentally in Ref.[19], where co-doping of anatase TiO_2 with nitrogen and chromium was found to improve the localization of the acceptor states, and reduce the effective optical gap. By replacing both Ti^{4+} and O^{2-} atoms with dopants in the same TiO_6 octahedral, it should be possible to "tune" the optical band gap to a much finer degree.

Whether calculated using RPBE, $I_p - E_a$ or G_0W_0, the energy gaps for both boron and nitrogen doped TiO_2 nanostructures are generally narrowed, as shown in 7(a) and (b). However, for nitrogen doped $(TiO_2)_n$ clusters where nitrogen acts as an acceptor ($n = 5, 6, 9$), the energy gap is actually *increased* when spin is conserved, compared to the undoped clusters in RPBE. This effect is not properly described by the $N \rightarrow N + 1$ transitions of $I_p - E_a$, for which spin is not conserved for these nitrogen doped clusters. On the other hand, when nitrogen acts as a donor ($n = 7, 8$) the smallest gap between energy levels does conserve spin.

The boron doped TiO_2 nanorods and nanotubes have perhaps the most promising energy gap results of the TiO_2 structures, as seen in 7(a). Boron dopants introduce in the nanorods localized occupied states near the conduction band edge in both RPBE (*cf.* 6) and G_0W_0 (*cf.* inset of 6) calculations. On the other hand, nitrogen doping of nanorods introduces well defined mid-gap states, as shown in 6. However, to perform water dissociation, the energy of the excited electron must be above that for hydrogen evolution, with respect to the vacuum level. This is not the case for such a mid-gap state. This opens the possibility of a second excitation from the mid-gap state to the conduction band. However, the cross section for such an excitation may be rather low.

For boron doping of 2D and 3D structures, the highest occupied state donates its electron almost entirely to the conduction band, yielding an n-type semiconductor. Thus at very low temperatures, the RPBE band gap is very small. The same is true for n-type nitrogen doped bulk anatase. For these reasons the energy gap between the highest fully occupied state and the conduction band, which may be more relevant for photoabsorption, is also shown. These RPBE gaps are still generally smaller than those for their undoped TiO_2 counterparts, shown in 5.

In summary, for both boron and nitrogen doped clusters we find RPBE gaps differ from $I_p - E_a$ by about 3 eV, while for nitrogen doped anatase the RPBE gap differs from experiment by about 0.6 eV. Given the common shift of 1 eV for undoped 2D and 3D structures, this suggests that both boron and nitrogen doped 2D TiO_2 structures are promising candidates for photocatalysis. Further, the boron and nitrogen doped 1D nanotube results also warrant further experimental investigation.
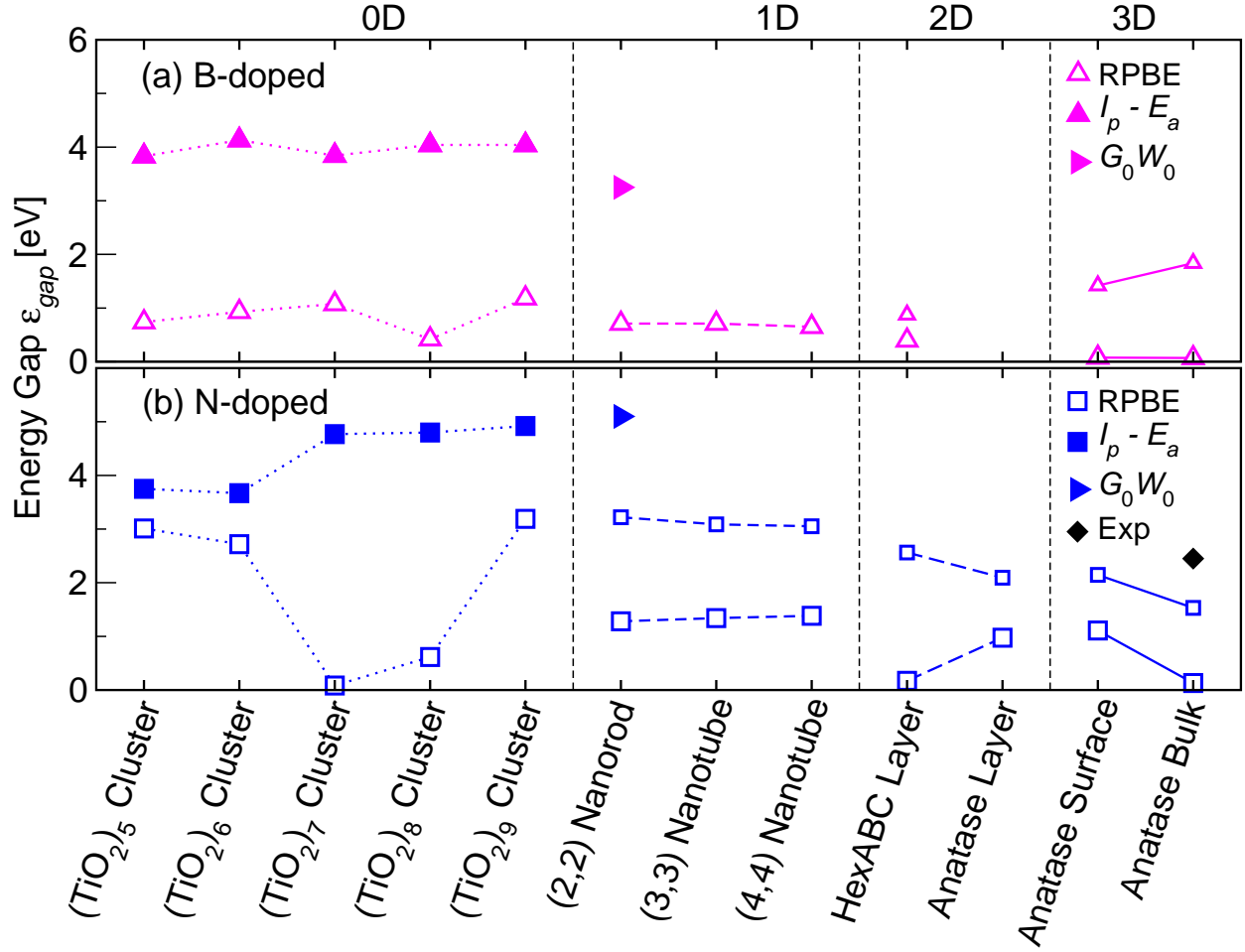
FIG. 7: Influence of doping on the energy gap ε_{gap} in eV versus TiO_2 structure for 0D $(TiO_2)_n$ clusters ($n \leq 9$), 1D TiO_2 (2,2) nanorods, (3,3) nanotubes, (4,4) nanotubes, 2D HexABC and anatase layers, and 3D anatase surface and bulk. The energy gaps for (a) boron doped systems from DFT calculations using the highest occupied and lowest unoccupied state gaps with the standard GGA RPBE xc-functional ($\triangle$) are compared with DFT $I_p - E_a$ calculations ($\blacktriangle$), and G_0W_0 quasi-particle calculations ($\blacktriangleright$), and (b) nitrogen doped systems from DFT calculations using the highest occupied and lowest unoccupied state gaps with the standard GGA RPBE xc-functional ($\square$) are compared with DFT $I_p - E_a$ calculations ($\blacksquare$), and G_0W_0 quasi-particle calculations ($\blacktriangleright$), and experimental ($\blacklozenge$) results[6,11,13,20,94]. Small open symbols denote transitions between highest fully occupied states and the conduction band.

VII. SOLAR CELLS FROM TIO$_2$ NANOSTRUCTURES: DYE-SENSITIZED SOLAR CELLS

TiO_2 is so far the most widely used solid material in the development of solar cell devices based on hybrid architectures[1,100]. In these devices, the dye, synthetic or organic, absorbs light,
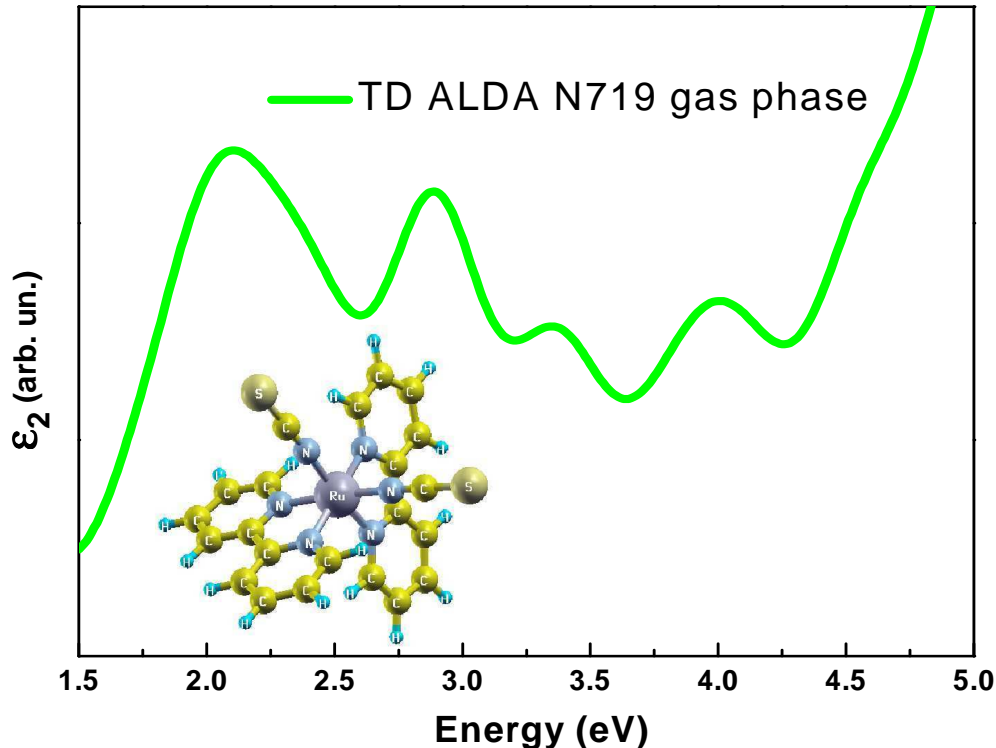
FIG. 8: Absorption spectrum calculated by TD Adiabatic LDA of the Ru-dye N719, whose structure is shown in the inset.

and electrons excited by the phonons are injected into the underlying oxide nanostructure. The hybrid system must therefore satisfy several requirements: (1) a proper absorption range for the dye, (2) a fast charge transfer in the oxide, (3) a slow back-transfer process, and (4) an easy collection and conduction of electrons in the oxide.

While absorption properties may be easily tuned at the chemical level by changing or adding functional groups, a critical point is to understand, and therefore control, the process at the interface. Indeed, simply having a good energy level alignment is not sufficient because the fast electron injection process is dynamical. Since the experimental characterization of complex systems (networks of nanostructures, with adsorbed dyes, and in solution) is quite complicated, the theoretical description of such systems can be of fundamental importance in unravelling the processes governing the behaviour of dye-sensitized solar cells (DSSC).

The most popular technique for studying these dynamical processes is time dependent DFT (TDDFT). For a detailed discussion of the success and possible limitations of this method when applied to hybrid systems, we refer the reader to Ref.[101]. TDDFT is a generalization of DFT which allows us to directly describe excited states. For example, it has previously been used successfully

to calculate the optical absorption of large organic molecules (8), such as Ru-dyes, or indolines. This same technique has also been applied recently to hybrid systems used for photovoltaic applications. We want here to highlight that the charge injection transfer has also been modelled for molecules adsorbed on TiO_2 clusters[102–111], giving estimations as fast as 8 fs for the injection time[107]. TDDFT is therefore a powerful tool to understand dynamical electronic effects in systems as large and complex as hybrid organic-oxide solar cells.

VIII. CONCLUSION

In this chapter we showed how an oxide of predominant importance in nanotechnological and environmental fields, such as photocatalysis and photovoltaics, can be successfully investigates by state-of-the-art *ab initio* techniques. The optical and excitonic properties of the bulk phases can be properly described by MBPT techniques. We also showed how the electronic properties of TiO_2 may be "tailored" using nanostructural changes in combination with boron and nitrogen doping. While boron doping tends to produce smaller band gap n-type semiconductors, nitrogen doping produces p-type or n-type semiconductors depending on whether or not nearby oxygen atoms occupy surface sites. This suggests that a p-type TiO_2 semiconductor may be produced using nitrogen doping in conjunction with surface confinement at the nanoscale. We also showed that it has been proved how, in the field of photovoltaics, TDDFT is a powerful tool to understand the mechanism of charge injection at organic-inorganic interfaces.

Palummo for helpful discussions.

[1] M. Grätzel, Photoelectrochemical cells, *Nature* **414**, 338–344 (2001).

[2] A. Heller, Hydrogen-evolving solar cells, *Science* **223**, 1141–1148 (1984).

[3] M. R. Hoffmann, S. T. Martin, W. Y. Choi, and D. W. Bahnmann, Environmental applications of semiconductor photocatalysis, *Chem. Rev.* **95**, 69–96 (1995).

[4] S. U. M. Khan, M. Al-Shahry, and W. B. I. Jr., Efficient photochemical water splitting by a chemically modified n-TiO$_2$, *Science* **297**, 2243–2245 (2002).

[5] Y. Gai, J. Li, S.-S. Li, J.-B. Xia, and S.-H. Wei, Design of narrow-gap TiO$_2$: A passivated codoping approach for enhanced photoelectrochemical activity, *Phys. Rev. Lett.* **102**, 036402–1–4 (2009).

[6] Z.-W. Qu and G.-J. Kroes, Theoretical study of the electronic structure and stability of titanium dioxide clusters (TiO$_2$)$_n$ with $n = 1$–9, *J. Phys. Chem. B* **110**, 8998–9007 (2006).

[7] H.-J. Zhai and L.-S. Wang, Probing the electronic structure and band gap eveolition of titanium oxide clusters (TiO$_2$)$_n^-$ ($n = 1$–10) using photoelectron spectroscopy, *J. Am. Chem. Soc.* **129**, 3022–3026 (2007).

[8] H. Imai, Y. Takei, K. Shimizu, M. Matsuda, and H. Hirashima, Direct preparation of anatase TiO$_2$ nanotubes in porous alumina membranes, *J. Mater. Chem.* **9**, 2971–2972 (1999).

[9] T. Kasuga, M. Hiramatsu, A. Hoson, T. Sekino, and K. Niihara, Titania nanotubes prepared by chemical processing, *Adv. Mater.* **11**, 1307–1311 (1999).

[10] G. Mogilevsky, Q. Chen, H. Kulkarni, A. Kleinhammes, W. M. Mullins, and Y. Wu, Layered nanostructures of delaminated anatase: Nanosheets and nanotubes, *J. Phys. Chem. C* **112**, 3239–3246 (2008).

[11] D. J. Mowbray, J. I. Martínez, J. M. García Lastra, K. S. Thygesen, and K. W. Jacobsen, Stability and electronic properties of TiO$_2$ nanostructures with and without B and N doping, *J. Phys. Chem. C* **113**, 12301–12308 (2009).

[12] S. In, A. Orlov, R. Berg, F. Carcía, S. Pedrosa-Jimenez, M. S. Tikhov, D. S. Wright, and R. M. Lambert, Effective visible light-activated B-doped and B,N-codoped TiO$_2$ photocatalysts, *J. Am. Chem. Soc.* **129**, 13790–13791 (2007).

[13] G. Liu, F. Li, D.-W. Wang, D.-M. Tang, C. Liu, X. Ma, G. Q. Lu, and H.-M. Cheng, Electron field emission of a nitrogen-doped TiO$_2$ nanotube array, *Nanotechnology* **19**, 025606–025611 (2008).

[14] R. Asahi, T. Morikawa, T. Ohwaki, K. Akoki, and Y. Taga, Visible-light photocatalysis in nitrogen-

doped titanium oxides, *Science* **298**, 269–271 (2001).

[15] A. Ghicov, J. M. Macak, H. Tsuchiya, J. Kunze, V. Hæublein, S. Kleber, and P. Schmuki, TiO_2 nanotube layers: Dose effects during nitrogen doping by ion implantation, *Chem. Phys. Lett.* **419**, 426–429 (2006).

[16] Y. Chen, S. Zhang, Y. Yu, H. Wu, S. Wang, B. Zhu, W. Huang, and S. Wu, Synthesis, characterization, and photocatalytic activity of N-doped TiO_2 nanotubes, *J. Disp. Sci. Tech.* **29**, 245–249 (2008).

[17] A. Nambu, J. Graciani, J. A. Rodriguez, Q. Wu, E. Fujita, and J. F. Sanz, N doping of TiO_2(110): Photoemission and density-functional studies, *J. Chem. Phys.* **125**, 094706–1–8 (2006).

[18] J. Graciani, L. J. Álvarez, J. A. Rodriguez, and J. F. Sanz, N doping of rutile TiO_2(110) surface. a theoretical DFT study, *J. Phys. Chem. C* **112**, 2624–2631 (2008).

[19] W. Zhu, X. Qiu, V. Iancu, X.-Q. Chen, H. Pan, W. Wang, N. M. Dimitrijevic, T. Rajh, H. M. M. III, M. P. Paranthaman, G. M. Stocks, H. H. Weitering, B. Gu, G. Eres, and Z. Zhang, Band gap narrowing of titanium oxide semiconductors by noncompensated anion-cation codoping for enhanced visible-light photoactivity, *Phys. Rev. Lett.* **103**, 226401–1–4 (2009).

[20] D. V. Bavykin, J. M. Friedrich, and F. C. Walsh, Protonates titanates and TiO_2 nanostructured materials: Synthesis, properties, and applications, *Adv. Mater.* **18**, 2807–2824 (2006).

[21] O. Khaselev and J. A. Turner, A monolithic photovoltaic-photoelectrochemical device for hydrogen production via water splitting, *Science* **280**, 425–427 (1998).

[22] M. K. Nazeeruddin, A. Kay, I. Rodicio, R. Humphry-Baker, E. Müller, P. Liska, N. Vlachopoulos, and M. Grätzel, Conversion of light to electricity by *cis*-X_2Bis(2,2'-bipyridyl-4,4'-dicarboxylate)ruthenium(ii) charge-transfer sensitizers (X = Cl^-, Br^-, I^-, CN^-, and SCN^-) on nanocrystalline TiO_2 electrodes, *J. Am. Chem. Soc.* **115**, 6382–6390 (1993).

[23] P. Wang, S. M. Zakeeruddin, J. E. Moser, R. Humphry-Baker, P. Comte, V. Aranyos, A. Hagfeldt, M. K. Nazeeruddin, and M. Grätzel, Stable new sensitizer with improved light harvesting for nanocrystalline dye-sensitized solar cells, *Adv. Mater.* **16**, 1806–1811 (2004).

[24] X. Chen and S. S. Mao, Titanium dioxide nanomaterials: Synthesis, properties, modifications, and applications, *Chem. Rev.* **107**, 2891–2959 (2007).

[25] D. F. Watson and G. J. Meyer, Electron injection at dye-sensitized semiconductor electrodes, *Ann. Rev. Phys. Chem.* **56**, 119–156 (2005).

[26] J.-J. Wu, G.-R. Chen, C.-C. Lu, W.-T. Wu, , and J.-S. Chen, Performance and electron transport properties of TiO_2 nanocomposite dye-sensitized solar cells, *Nanotechnology* **19**, 105702–105708 (2008).

27 S. H. Kang, S.-H. Choi, M.-S. Kang, J.-Y. Kim, H.-S. Kim, T. Hyeon, and Y.-E. Sung, Nanorod-based dye-sensitized solar cells with improved charge collection efficiency, *Adv. Mater.* **20**, 54–58, (2008).

28 M. Adachi, Y. Murata, J. Takao, J. Jiu, M. Sakamoto, and F. Wang, Highly efficient dye-sensitized solar cells with a titania thin-film electrode composed of a network structure of single-crystal-like TiO_2 nanowires made by the "oriented attachment" mechanism, *J. Am. Chem. Soc.* **126**, 14943–14949 (2004).

29 M. V. Ganduglia-Pirovano, A. Hofmann, and J. Sauer, Oxygen vacancies in transition metal and rare earth oxides: Current state of understanding and remaining challenges, *Surf. Sci. Rep.* **62**, 219–270, (2007).

30 M. Gatti, F. Bruneval, V. Olevano, and L. Reining, Understanding correlations in vanadium dioxide from first principles, *Phys. Rev. Lett.* **99**, 266402–1–4 (2007).

31 P. Krüger, S. Bourgeois, B. Domenichini, H. Magnan, D. Chandesris, P. L. Fèvre, A. M. Flank, J. Jupille, L. Floreano, A. Cossaro, A. Verdini, and A. Morgante, Defect states at the TiO_2(110) surface probed by resonant photoelectron diffraction, *Phys. Rev. Lett.* **100**, 055501–1–4 (2008).

32 C. Di Valentin, G. Pacchioni, and A. Selloni, Electronic structure of defect states in hydroxylated and reduced rutile TiO_2(110) surfaces, *Phys. Rev. Lett.* **97**, 166803–1–4 (2006).

33 T. Minato, Y. Sainoo, Y. Kim, H. S. Kato, K. ichi Aika, M. Kawai, J. Zhao, H. Petek, T. Huang, W. He, B. Wang, Z. Wang, Y. Zhao, J. Yang, and J. G. Hou, The electronic structure of oxygen atom vacancy and hydroxyl impurity defects on titanium dioxide (110) surface, *J. Chem. Phys.* **130**, 124502–1–11 (2009).

34 E. Finazzi, C. D. Valentin, G. Pacchioni, and A. Selloni, Excess electron states in reduced bulk anatase TiO_2: Comparison of standard GGA, GGA + U, and hybrid DFT calculations, *J. Chem. Phys.* **129**, 154113–1–9 (2008).

35 G. Pacchioni, Modeling doped and defective oxides in catalysis with density functional theory methods: Room for improvements, *J. Chem. Phys.* **128**, 182505–1–10 (2008).

36 V. M. Khomenko, K. Langer, H. Rager, and A. Fett, Electronic absorption by Ti^{3+} ions and electron delocalization in synthetic blue rutile, *Phys. Chem. Minerals* **25**, 338–346 (1998).

37 S. Wendt, P. T. Sprunger, E. Lira, G. K. H. Madsen, Z. Li, J. O. Hansen, J. Matthiesen, A. Blekinge-Rasmussen, E. Laegsgaard, B. Hammer, and F. Besenbacher, The Role of Interstitial Sites in the Ti3d Defect State in the Band Gap of Titania, *Science* **320**, 1755–1759, (2008).

38 L. Hedin, New method for calculating the one-particle Green's function with application to the electron-gas problem, *Phys. Rev.* **139**, A796–A823 (1965).

[39] R. M. Dreizler and E. K. U. Gross, *Density Functional Theory* (Springer Verlag, Heidelberg, 1990).

[40] L. Fetter and J. D. Walecka, *Quantum theory of Many Body Systems* (McGraw-Hill, New York, 1981).

[41] P. Hohenberg and W. Kohn, Inhomogeneous electron gas, *Phys. Rev.* **136**, B864–B871 (1964).

[42] W. Kohn and L. J. Sham, Self-consistent equations including exchange and correlation effects, *Phys. Rev.* **140**, A1133–A1138, (1965).

[43] D. M. Ceperley and B. J. Alder, Ground state of the electron gas by a stochastic method, *Phys. Rev. Lett.* **45**, 566–569, (1980).

[44] J. P. Perdew and A. Zunger, Self-interaction correction to density-functional approximations for many-electron systems, *Phys. Rev. B* **23**, 5048–5079 (1981).

[45] J. P. Perdew, K. Burke, and M. Ernzerhof, Generalized gradient approximation made simple, *Phys. Rev. Lett.* **77**, 3865–3868 (1996).

[46] C. Adamo and V. Barone, Toward reliable density functional methods without adjustable parameters: The pbe0 model, *J. Chem. Phys.* **110**, 6158–6170 (1999).

[47] A. D. Becke, Density-functional thermochemistry. iii. the role of exact exchange, *J. Chem. Phys.* **98**, 5648–5652 (1993).

[48] J. P. Perdew and M. Levy, Physical content of the exact Kohn-Sham orbital energies: Band gaps and derivative discontinuities, *Phys. Rev. Lett.* **51**, 1884–1887 (1983).

[49] R. D. Mattuck, *A Guide to Feynman Diagrams in the Many-Body Problem* (McGraw-Hill, New York, 1976).

[50] L. Hedin and S. Lundqvist. "Effects of Electron-Electron and Electron-Phonon Interactions on the One-Electron States of Solids," in *Solid State Physics*, Vol. **23**, edited by H. Ehrenreich, F. Seitz, and D. Turnbull (Academic Press, New York, 1969) pp. 1–181.

[51] G. Strinati, Application of the Green's functions method to the study of the optical properties of semiconductors, *Rivista Nuovo Cimento* **11**, 1–86 (1988).

[52] P. M. Echenique, J. M. Pitarke, E. V. Chulkov, and A. Rubio, Theory of inelastic lifetimes of low-energy electrons in metals, *Chem. Phys.* **251**, 1–35 (2000).

[53] M. S. Hybertsen and S. G. Louie, Electron correlation in semiconductors and insulators: Band gaps and quasiparticle energies, *Phys. Rev. B* **34**, 5390–5413 (1986).

[54] R. W. Godby, M. Schlüter, and L. J. Sham, Self-energy operators and exchange-correlation potentials in semiconductors, *Phys. Rev. B* **37**, 10159–10175 (1988).

[55] S. L. Adler, Quantum theory of the dielectric constant in real solids, *Phys. Rev.* **126**, 413–420 (1962).

[56] J. Lindhard, On the properties of a gas of charged particles, *Mat. Fys. Medd. K. Dan. Vidensk. Selsk.* **28**, 1–57 (1954).

[57] G. Onida, L. Reining, and A. Rubio, Electronic excitations: density-functional versus many-body Green's-function approaches, *Rev. Mod. Phys.* **74**, 601–659 (2002).

[58] P. J. Hardmand, G. N. Raikar, C. A. Muryn, G. van der Laan, P. L. Wincott, G. Thornton, D. W. Bullett, and P. A. D. M. A. Dale, Valence-band structure of TiO_2 along the Γ-Δ-X and Γ-Σ-M directions, *Phys. Rev. B* **49**, 7170–7177 (1994).

[59] S. Eriksen and R. G. Egdell, Electronic excitations at oxygen deficient $TiO_2(110)$ surfaces: A study by EELS, *Surf. Sci.* **180**, 263–278 (1987).

[60] R. Heise, R. Courths, and S. Witzel, Valence band densities-of-states of $TiO_2(110)$ from resonant photoemission and photoelectron diffraction, *Solid State Commun.* **84**, 599–602 (1992).

[61] R. G. Egdell, S. Eriksen, and W. R. Flavell, Oxygen deficient SnO_2 (110) and TiO_2 (110): A comparative study by photoemission, *Solid State Commun.* **60**, 835–838 (1986).

[62] R. L. Kurtz, R. Stock-Bauer, T. E. Madey, E. Román, and J. L. D. Segovia, Synchrotron radiation studies of H_2O adsorption on $TiO_2(110)$, *Surf. Sci.* **218**, 178–200 (1989).

[63] R. G. Breckenridge and W. R. Hosler, Electrical properties of titanium dioxide semiconductors, *Phys. Rev.* **91**, 793–802 (1953).

[64] F. Arntz and Y. Yacoby, Electroabsorption in rutile TiO_2, *Phys. Rev. Lett.* **17**, 857–860 (1966).

[65] A. Frova, P. J. Boddy, and Y. S. Chen, Electromodulation of the optical constants of rutile in the UV, *Phys. Rev.* **157**, 700–708 (1967).

[66] A. K. Ghosh, F. G. Wakim, and R. R. Addiss, Photoelectronic processes in rutile, *Phys. Rev.* **184**, 979–988 (1969).

[67] A. Amtout and R. Leonelli, Optical properties of rutile near its fundamental band gap, *Phys. Rev. B* **51**, 6842–6851 (1995).

[68] S. Hüfner and G. K. Wertheim, Core-electron splittings and hyperfine fields in transition-metal compounds, *Phys. Rev. B* **7**, 2333–2336 (1973).

[69] D. W. Fischer, X-ray band spectra and molecular-orbital structure of rutile TiO_2, *Phys. Rev. B* **5**, 4219–4226 (1972).

[70] F. M. F. de Groot, J. Faber, J. J. M. Michiels, M. T. Czyżyk, M. Abbate, and J. C. Fuggle, Oxygen $1s$ x-ray absorption of tetravalent titanium oxides: A comparison with single-particle calculations, *Phys. Rev. B* **48**, 2074–2080 (1993).

[71] L. A. Grunes, Study of the k edges of $3d$ transition metals in pure and oxide form by x-ray-absorption spectroscopy, *Phys. Rev. B* **27**, 2111–2131 (1983).

[72] G. van der Laan, Polaronic satellites in x-ray-absorption spectra, *Phys. Rev. B* **41**, 12366–12368 (1990).

[73] F. M. F. de Groot, M. Grioni, J. C. Fuggle, J. Ghijsen, G. A. Sawatzky, and H. Petersen, Oxygen 1s x-ray-absorption edges of transition-metal oxides, *Phys. Rev. B* **40**, 5715–5723 (1989).

[74] K. Watanabe, K. Inoue, and F. Minami, Resonant phenomena of hyper-raman-scattering of optic phonons in a TiO_2 crystal, *Phys. Rev. B* **46**, 2024–2033 (1992).

[75] D. C. Cronemeyer, Electrical and optical properties of rutile single crystals, *Phys. Rev.* **87**, 876–886 (1952).

[76] L. Kavan, M. Grätzel, S. E. Gilbert, C. Klemenz, and H. J. Scheel, Electrochemical and photoelectrochemical investigation of single-crystal anatase, *J. Am. Chem. Soc.* **118**, 6716–6723 (1996).

[77] L. Fleming, C. C. Fulton, G. Lucovsky, J. E. Rowe, M. D. Ulrich, and J. Lüning, Local bonding analysis of the valence and conduction band features of TiO_2, *J. Appl. Phys.* **102**, 033707–1–7 (2007).

[78] R. Sanjinés, H. Tang, H. Berger, F. Gozzo, G. Margaritondo, and F. Lévy, Electronic structure of anatase TiO_2 oxide, *J. Appl. Phys.* **75**, 2945–2951 (1994).

[79] H. Tang, K. Prasad, R. Sanjinès, P. E. Schmid, and F. Lévy, Electrical and optical properties of TiO_2 anatase thin films, *J. Appl. Phys.* **75**, 2042–2047 (1994).

[80] M. Cardona and G. Harbeke, Optical properties and band structure of wurtzite-type crystals and rutile, *Phys. Rev.* **137**, A1467–A1476 (1965).

[81] J. Pascual, J. Camassel, and H. Mathieu, Fine structure in the intrinsic absorption edge of TiO_2, *Phys. Rev. B* **18**, 5606–5614 (1978).

[82] N. Hosaka, T. Sekiya, M. Fujisawa, C. Satoko, and S. Kurita, Uv reflection spectra of anatase TiO_2, *J. Electron Spec. Rel. Phen.* **78**, 75–78 (1996).

[83] N. Hosaka, T. Sekiya, C. Satoko, and S. Kurita, Optical properties of single-crystal anatase TiO_2, *J. Phys. Soc. Jpn.* **66**, 877–880 (1997).

[84] H. Tang, F. Lévy, H. Berger, and P. E. Schmid, Urbach tail of anatase TiO_2, *Phys. Rev. B* **52**, 7771–7774 (1995).

[85] M. van Schilfgaarde, T. Kotani, and S. Faleev, Quasiparticle self-consistent GW theory, *Phys. Rev. Lett.* **96**, 226402–1–4, (2006).

[86] F. Labat, P. Baranek, C. Doman, C. Minot, and C. Adamo, Density functional theory analysis of the structural and electronic properties of TiO_2 rutile and anatase polytypes: Performances of different

exchange-correlation functionals, *J. Chem. Phys.* **126**, 154703–1–12, (2007).

[87] J. Muscat, A. Wander, and N. M. Harrison, On the prediction of band gaps from hybrid functional theory, *Chem. Phys. Lett.* **342**, 397–401 (2001).

[88] U. Diebold, The surface science of titanium dioxide, *Surf. Sci. Rep.* **48**, 53–229 (2003).

[89] L. Chiodo, J. M. García-Lastra, A. Incomino, H. Petek, S. Ossicini, and A. Rubio. *Ab initio* electronic and optical description of TiO$_2$ crystalline phases: Towards photocatalysis and photovoltaic applications. (unpublished, 2009).

[90] J. Muscat, V. Swamy, and N. Harrison, First-principles calculations of the phase stability of TiO$_2$, *Phys. Rev. B* **65**, 224112–1–15 (2002).

[91] M. Oshikiri, M. Boero, J. Ye, F. Aryasetiawan, and G. Kido, The electronic structures of the thin films of InVO$_4$ and TiO$_2$ by first principles calculations, *Thin Solid Films* **445**, 168–174 (2003).

[92] R. Asahi, Y. Taga, W. Mannstadt, and A. J. Freeman, Electronic and optical properties of anatase TiO$_2$, *Phys. Rev. B* **61**, 7459–7465 (2000).

[93] M. Calatayud, P. Mori-Sánchez, A. Beltrán, A. Martín Pendás, E. Francisco, J. Andrés, and J. M. Recio, Quantum-mechanical analysis of the equation of state of anatase TiO$_2$, *Phys. Rev. B* **64**, 184113–1–9 (2001).

[94] L. Thulin and J. Guerra, Calculations of strain-modified anatase TiO$_2$ band structures, *Phy. Rev. B* **77**, 195112–1–5, (2008).

[95] H. M. Lawler, J. J. Rehr, F. Vila, S. D. Dalosto, E. L. Shirley, and Z. H. Levine, Optical to UV spectra and birefringence of SiO$_2$ and TiO$_2$: First-principles calculations with excitonic effects, *Phys. Rev. B* **78**, 205108–1–8 (2008).

[96] Z.-L. Cai, K. Sendt, and J. R. Reimers, Failure of density-functional theory and time-dependent density-functional theory for large extended π systems, *J. Chem. Phys* **117**, 5543–5549 (2002).

[97] U. Salzner, J. B. Lagowski, P. G. Pickup, and R. A. Poirier, Design of low band gap polymers employing density functional theory – hybrid functionals ameliorate band gap problem, *J. Comput. Chem.* **18**, 1943–1953 (1997).

[98] F. De Angelis, A. Tilocca, and A. Selloni, Time-dependent dft study of [Fe(CN)$_6$]$^{4-}$ sensitization of TiO$_2$ nanoparticles, *J. Am. Chem. Soc.* **126**, 15024–15025 (2004).

[99] B. Hammer, L. B. Hansen, and J. K. Norskov, Improved adsorption energetics with density functional theory using revised Perdew-Burke-Ernzerhof functionals, *Phys. Rev. B* **59**, 7413–7421 (1999).

[100] M. Gratzel, Dye-sensitized solar cells, *J. Photochem. Photobiol. C–Photochem. Rev.* **4**, 145–153 (2003).

[101] M. A. L. Marques, C. Ullrich, F. Nogueira, A. Rubio, K. Burke, and E. Gross, Eds., *Time-Dependent Density Functional Theory*, Vol. **706**, (Springer, Berlin, 2006).

[102] F. De Angelis, A. Tilocca, and A. Selloni, Time-dependent DFT study of [Fe(CN)(6)](4-) sensitization of TiO_2 nanoparticles, *J. Am. Chem. Soc.* **126**, 15024–15025 (2004).

[103] F. De Angelis, S. Fantacci, A. Selloni, and M. Nazeeruddin, Time dependent density functional theory study of the absorption spectrum of the $[Ru(4,4'\text{-}COO^--2,2'\text{-}bpy)_2(X)_2]^{4-}$ (X = NCS, Cl) dyes in water solution, *Chem. Phys. Lett.* **415**, 115–120, (2005).

[104] M. Nazeeruddin, F. De Angelis, S. Fantacci, A. Selloni, G. Viscardi, P. Liska, S. Ito, B. Takeru, and M. Gratzel, Combined experimental and DFT-TDDFT computational study of photoelectrochemical cell ruthenium sensitizers, *J. Am. Chem. Soc.* **127**, 16835–16847 (2005).

[105] F. De Angelis, S. Fantacci, A. Selloni, M. K. Nazeeruddin, and M. Gratzel, Time-dependent density functional theory investigations on the excited states of Ru(II)-dye-sensitized TiO_2 nanoparticles: The role of sensitizer protonation, *J. Am. Chem. Soc.* **129**, 14156–14157 (2007).

[106] F. De Angelis, S. Fantacci, and A. Selloni, Alignment of the dye's molecular levels with the TiO_2 band edges in dye-sensitized solar cells: a DFT-TDDFT study, *Nanotechnology* **19**, 424002–1–7 (2008).

[107] W. R. Duncan, W. M. Stier, and O. V. Prezhdo, *Ab initio* nonadiabatic molecular dynamics of the ultrafast electron injection across the alizarin-TiO_2 interface, *J. Am. Chem. Soc.* **127**, 7941–7951 (2005).

[108] W. R. Duncan and O. V. Prezhdo, Theoretical studies of photoinduced electron transfer in dye-sensitized TiO_2, *Ann. Rev. Phys. Chem.* **58**, 143–184 (2007).

[109] W. R. Duncan, C. F. Craig, and O. V. Prezhdo, Time-domain *ab initio* study of charge relaxation and recombination in dye-sensitized TiO_2, *J. Am. Chem. Soc.* **129**, 8528–8543 (2007).

[110] O. V. Prezhdo, W. R. Duncan, and V. V. Prezhdo, Dynamics of the photoexcited electron at the chromophore-semiconductor interface, *Acc. Chem. Res.* **41**, 339–348 (2008).

[111] W. R. Duncan and O. V. Prezhdo, Temperature independence of the photoinduced electron injection in dye-sensitized TiO_2 rationalized by *ab initio* time-domain density functional theory, *J. Am. Chem. Soc.* **130**, 9756–9762 (2008).